

Sliding DFT-based Signal Recovery for Modulo ADC with 1-bit Folding Information

Neil Irwin Bernardo, *Member, IEEE*

Abstract—The modulo analog-to-digital converter (ADC) is a promising solution to resolve the limited dynamic range (DR) issue of conventional ADCs and achieve an enhanced digital resolution given a fixed quantization bit budget. However, a modulo ADC requires an unfolding scheme to correct the nonlinear distortion introduced by the modulo operation. This paper presents a sliding discrete Fourier Transform (DFT)-based method for fast signal reconstruction given the modulo ADC output sequence and a 1-bit folding information sequence. In contrast to existing DFT-based signal recovery techniques for modulo ADCs, our proposed sliding DFT method reduces the required observation time and minimizes the spectral leakage effects via proper choice of window function parameters. A mean squared error (MSE) performance guarantee is established for the proposed signal recovery algorithm. More precisely, we derive sufficient conditions for the oversampling factor (OF) and the number of quantization bits (b) to obtain a specific MSE performance. Our numerical results demonstrate that modulo ADCs equipped with our proposed recovery method can outperform conventional ADCs without modulo for $OF \geq 4$ and $b \geq 4$. Moreover, the proposed sliding DFT-based recovery method outperforms higher-order difference-based recovery in terms of MSE, particularly in the low-sampling-rate and low-resolution regime. The impact of spectral leakage on the MSE performance of the proposed sliding DFT recovery method is also quantified.

Index Terms—Modulo ADC, Sampling, Quantization, Sliding DFT, Reconstruction.

I. INTRODUCTION

An analog-to-digital converter (ADC) is a critical element of data acquisition systems since it is responsible for the transformation of continuous-time analog observations from the physical world into some format that can be further processed or stored in digital signal processing (DSP) pipelines. The conversion process in conventional ADCs involves two operations: (1) a *sampler* that acquires the amplitude of the continuous-time input at uniform time intervals, and (2) a *quantizer* that maps the amplitude samples into a finite set of discrete values [1]. The sampling rate and quantizer resolution of an ADC are chosen according to some fidelity criterion and power consumption budget. Theoretically, the sampling rate requirement for alias-free reconstruction and the quantization resolution needed to achieve some distortion level are governed by the Shannon-Nyquist sampling theorem [2] and the rate-distortion theory [3], respectively. However,

increasing these parameters also incurs a substantial increase in the ADC power consumption. More precisely, the ADC power consumption scales exponentially with the number of quantization bits and scales linearly with the sampling rate [4].

Another important parameter that affects the performance of an ADC is the dynamic range (DR). Due to the finite number of quantization bits in an ADC, a trade-off exists between its dynamic range and its resolution. An input signal may drive the ADC into saturation if the DR of the input signal far exceeds the DR of the ADC. However, increasing the ADC range to accommodate high DR signals would increase the quantization step size. Weak input signals could be buried in the quantization noise. The presence of both weak and strong components in the input signal increases the required ADC resolution to achieve a specific fidelity criterion [5].

A promising solution to address the DR bottleneck of ADCs is the *modulo sampling* framework [6], [7]. The idea in modulo sampling is to apply a nonlinear folding operation called *modulo* to the input signal before the ADC. This modulo pre-processing stage ensures that the signal range is confined within the DR of the ADC. Moreover, for a given amplitude quantization bit budget, modulo ADCs can achieve better digital resolution compared to conventional ADCs as demonstrated in prior works [8], [9].

Since modulo operation intentionally introduces nonlinear distortion to the signal, several studies on modulo sampling have focused on the development of robust recovery techniques to correct the distortion induced by the modulo operation. Reconstruction techniques for modulo sampling include higher-order differences-based approaches [7], discrete Fourier transform (DFT)-based techniques [10]–[15], prediction-based filtering [16], [17], iterative methods [18], sparse signal modulo recovery [19]–[22], multi-channel modulo structures [23]–[26], and thresholding-based schemes [27]–[31]. There are also research efforts geared toward the practical hardware implementation of modulo ADCs [10], [32]–[36] and their potential applications in radars, communication systems, imaging, and electroencephalogram (EEG) recovery [12], [25], [37]–[46].

Another important research direction in modulo ADC is the establishment of theoretical performance guarantees to reconstruct the unfolded signal from modulo samples. In [7], it is shown that the higher-order differences-based reconstruction approach can perfectly reconstruct a finite-energy bandlimited (BL) signal from its modulo samples if the sampling rate used is at least $2\pi e$ (≈ 17.07) times the Nyquist rate. This sufficient condition for the sampling rate increases significantly in the presence of bounded noise [7, Theorem 3]. For finite-energy BL signals, perfect reconstruction is possible for any sampling rate approaching the Nyquist rate from above by

N.I. Bernardo is with the Electrical and Electronics Engineering Institute, University of the Philippines Diliman, Quezon City 1101, Philippines (e-mail: neil.bernardo@eee.upd.edu.ph).

This author acknowledges the Office of the Chancellor of the University of the Philippines Diliman, through the Office of the Vice Chancellor for Research and Development, for funding support through the PhD Incentive Award Grant 252509 YEAR 1.

using a prediction filter with sufficiently long filter length [16]. This approach does not need any side information such as knowledge of unfolded samples and auto-correlation function. However, the proposed prediction filter-based approach did not take into account the impact of finite quantization. Theoretical guarantees for Fourier-based reconstruction had been established in [10]. However, this approach suffers from spectral leakage and may require long observation windows. To avoid spectral leakage, recovery methods based on time-domain thresholding can also be used. Such methods work for generalized modulo sampling models which consider the modulo hysteresis and the folding transients. However, recovery guarantees of thresholding-based recovery fail under ideal modulo nonlinearities. This is explained in Section III-E. The recently developed UNO framework [47] integrates the Unlimited Sampling Framework (USF) [7] with 1-bit quantization, where each folded sample is processed by multiple 1-bit quantizers using varying thresholds. In effect, the set of 1-bit quantizers operates collectively as a multi-bit quantizer. Furthermore, the accompanying theoretical guarantees are expressed through high-probability bounds.

A recent work on modulo ADCs with 1-bit side information [14], [48] established a mean squared error (MSE) performance guarantee when the oversampling factor (OF) is above three and the number of quantization bits is above three. The 1-bit side information identifies the indices in which folding occurred. However, the proofs neglected the spectral leakage effects and the contribution of quantization noise at certain time indices. When the 1-bit folding information is not available in the recovery process, the same MSE guarantees can be achieved by an orthogonal matching pursuit (OMP)-based recovery scheme [48]. However, the sufficient condition for the amplitude quantization bit budget becomes stricter.

In this work, we propose a sliding DFT approach to construct the original input samples from the modulo ADC output samples and an additional 1-bit folding information signal. The recovery procedure uses short-time Fourier transform (STFT) to facilitate successive frame-based unfolding of the modulo samples. To significantly reduce the impact of spectral leakage in STFT computation, a window function with smooth transitions at the edges is multiplied to the frame. A MSE performance guarantee for the proposed recovery method is also established and is compared with the simulated MSE results. Effectively, the use of sliding DFT-based recovery solves the high computational complexity issue of the Fourier-based recovery with 1-bit folding information presented in [14], [48].

The main contributions of this work are summarized as follows:

- We develop an unfolding algorithm for modulo ADC output with 1-bit folding information signal based on sliding-window DFT. In contrast to existing Fourier-based reconstruction techniques, the proposed algorithm does not need a long observation window to process the modulo ADC output. This significantly reduces the computational complexity of the recovery algorithm. Furthermore, spectral leakage due to the short frame observations can be reduced by choosing an appropriate window function.

The computational complexity of the proposed recovery algorithm is derived in Section III-G.

- We establish sufficient conditions for the oversampling factor (OF) and quantizer resolution (b) of the modulo ADC so that the proposed recovery algorithm can correctly unfold the modulo ADC output. Under these conditions, only the quantization noise contributes to the MSE. The MSE performance guarantee of the sliding DFT-based recovery is derived in Theorem 1.
- We compare the MSE of the modulo ADC equipped with our proposed recovery procedure to that of the conventional ADC, i.e., no modulo operation, and that of modulo ADC equipped with higher-order differences (HoD)-based recovery method. Under the established sufficient conditions, we show that the MSE of the modulo ADC which uses the sliding DFT recovery algorithm is in $\mathcal{O}\left(\frac{1}{\text{OF}^3}\right)$ when spectral leakage is neglected and is in $\mathcal{O}\left(\frac{1}{\text{OF}^2}\right)$ otherwise. The parameter OF is the oversampling factor to be defined in Section II. Meanwhile, the MSE of a conventional ADC is in $\mathcal{O}\left(\frac{1}{\text{OF}}\right)$. We also note that the HoD-based recovery method fails to unfold the modulo ADC output at certain values of OF when $b = 4, 5$. Numerical results are presented to demonstrate these behaviors.

Notation: The following notations are used throughout the paper. The sets of real numbers, integers, and natural numbers are denoted as \mathbb{R} , \mathbb{Z} , and \mathbb{N} , respectively. When referring to discrete-time signals, the notation $z[n]$ is used to signify $z(nT_s)$, assuming that the sampling period T_s is evident from the context. The first-order difference of a discrete-time signal $x[n]$ is denoted as $\underline{x}[n] = x[n] - x[n-1]$, where $x[-1] = 0$ unless stated otherwise. Vectors and matrices are written in bold format (e.g., \mathbf{z} , \mathbf{A}) while sets are written in calligraphic format (e.g., \mathcal{S}). The cardinality of a set \mathcal{S} is written as $|\mathcal{S}|$. If \mathbf{x} is a vectorized form of some discrete-time signal $x[n]$, then $\underline{\mathbf{x}}$ is the vectorized form of $\underline{x}[n]$. The ℓ_p -norm of a vector \mathbf{x} is written as $\|\mathbf{x}\|_p$. The set of values of the discrete-time signal $x[n]$ for $n \in \mathcal{S}$ is denoted as $x_{\mathcal{S}}[n]$. The Moore-Penrose inverse of a matrix $\mathbf{A} \in \mathbb{R}^{m \times n}$ is denoted by \mathbf{A}^\dagger . We use ω and Ω to denote the frequencies for the continuous-time Fourier Transform (CTFT) and discrete-time Fourier Transform (DTFT) spectrum, respectively. We also use the standard Big-O notation $\mathcal{O}(\cdot)$ to describe asymptotic growth rates in this paper.

II. SYSTEM MODEL AND RECONSTRUCTION ALGORITHM

A. Signal Acquisition Process

We consider the modulo ADC system shown in Figure 1. The input $f(t)$ is a bandlimited signal with (angular) frequency support $[-\frac{\omega_m}{2}, +\frac{\omega_m}{2}]$. This signal is folded by the modulo operator block to produce the modulo signal $f_{\lambda'}(t)$. The operation behind the modulo folding mechanism is shown in Figure 2. This feedback structure for the folding operation is adopted from [34]. Comparator 1 triggers a positive value whenever $f_{\lambda'}(t)$ crosses $+\lambda$ from below. Similarly, comparator 2 triggers a negative value whenever $f_{\lambda'}(t)$ crosses $-\lambda$ from above. These trigger signals are fed to a discrete voltage

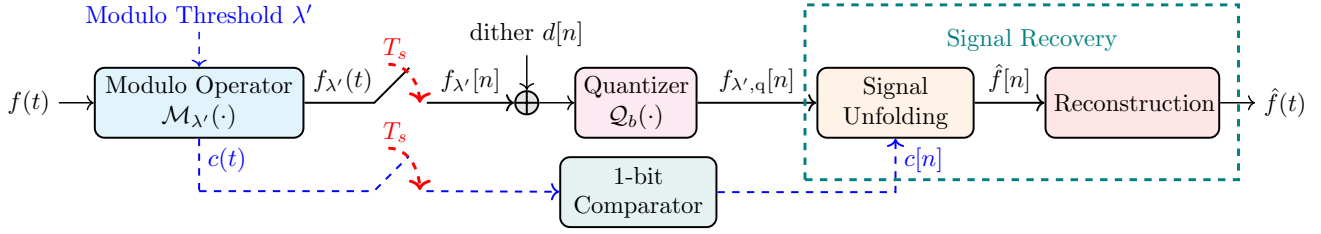


Fig. 1. The schematic diagram of the modulo ADC with 1-bit folding information. The 1-bit folding information $c[n]$ is obtained by sampling $c(t)$.

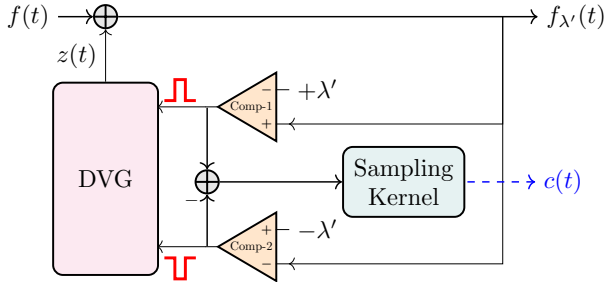


Fig. 2. The folding mechanism and folding information generation of the modulo operator block.

generator (DVG). The voltage level of the DVG is increased (resp. decreased) by $2\lambda'$ whenever it receives a positive (resp. negative) trigger signal. A detailed circuit-level implementation of the DVG is presented in [34]. Mathematically, the folded signal can be expressed as

$$f_{\lambda'}(t) = \left[(f(t) + \lambda') \bmod 2\lambda' \right] - \lambda', \quad (1)$$

where $\lambda' \in (0, \|f(t)\|_{\infty})$ is the modulo threshold. The ℓ_{∞} -norm of a waveform is its maximum amplitude. Throughout this paper, we assume ideal modulo nonlinearities. That is, there are no modulo hysteresis and folding transients like in the generalized modulo sampling model presented in [28]. Furthermore, we also assume that the amplitude of the first sample of $f(t)$, i.e. $f[0]$, is within $[-\lambda', \lambda']$. This ensures that no unknown constant offset $2\lambda'p$, where $p \in \mathbb{Z}$, is present in the reconstructed signal.

To digitize the modulo signal, $f_{\lambda'}(t)$ is first sampled at every T_s seconds. The angular sampling rate is $\omega_s = \frac{2\pi}{T_s} = \text{OF} \times \omega_m$, where $\text{OF} \geq 1$ is the oversampling factor. We also define $\rho = \frac{1}{\text{OF}}$. Prior to quantization, a (non-subtractive) dither sequence $d[n]$ is added to $f_{\lambda'}[n]$. Samples of the dither sequence are drawn i.i.d. from a triangle distribution with amplitude support $(-\frac{2\lambda}{2^b}, +\frac{2\lambda}{2^b})$. The rationale for using triangle dither in the modulo ADC problem setup is explained in Section III-B. The resulting signal is then forwarded to the b -bit uniform scalar quantizer $Q_b(\cdot)$ with range $[-\lambda, +\lambda]$. Consequently, each quantization bin has width $\frac{2\lambda}{2^b}$. To prevent the quantizer from being overloaded, the quantizer DR is set to $\lambda = \frac{2^b \lambda'}{2^b - 2}$. The quantizer output can be written as

$$f_{\lambda',q}[n] = Q_b(f_{\lambda'}[n] + d[n]) = f[n] + z[n] + \epsilon[n], \quad (2)$$

where $z[n] = f_{\lambda'}[n] - f[n] \in 2\lambda'\mathbb{Z}$ is the residual samples due to the folding operation and $\epsilon[n] = Q_b(f_{\lambda'}[n] + d[n]) - f_{\lambda'}[n]$ is the quantization noise sequence.

In addition to $f_{\lambda'}(t)$, the modulo operator also generates a signal $c(t)$ according to Figure 2. This signal is a finite rate of innovation (FRI) signal and can be expressed as

$$c(t) = g_2(t) * \left(\sum_k g_1(t - \tau_k) \right) = \sum_k g(t - \tau_k),$$

where τ_k is the location of the level crossings, $g_1(t)$ is the pulse shape of the trigger signals, $g_2(t)$ is the sampling kernel, and $g(t) = (g_2 * g_1)(t)$. To simplify the analysis, $g(t)$ is assumed to be a rectangular pulse with width T_s and unity amplitude. The signal $c(t)$ is sampled at rate ω_s and then fed to a 1-bit comparator to produce $c[n]$. In essence, $c[n]$ provides information if the signal crossed either $+\lambda'$ or $-\lambda'$ in the interval $(nT_s, (n+1)T_s)$. We note that even though our modulo ADC generates two channel streams, our setup is different from the multichannel modulo sampling structures presented in [23]–[25]. The multiple channels in [23]–[25] use different modulo thresholds to process the same signal, thereby generating two multi-bit modulo ADC output sample streams. In contrast, our second stream only indicates the position of the folding instances in the first stream. The information carried by this second stream can be represented by a single bit per sample.

B. Is the 1-bit Folding Information Practical?

One might wonder if generating 1-bit folding information $c[n]$ is practical when implementing a modulo ADC. Early works on modulo ADC hardware have considered recovery methods that utilize the reset count in addition to the self-reset ADC output samples [49], [50]. However, implementing a self-reset ADC with a multi-bit reset count signal may incur a significant increase in power consumption and circuit complexity if the threshold is small [7]. Furthermore, having a multi-bit reset count signal that has the same resolution as the self-reset ADC output samples doubles the storage requirements of the system. Limiting $c[n]$ to 1-bit solves these problems. As shown in Figures 1 and 2, generating $c[n]$ would only require one additional comparator and one adder from the “no $c[n]$ ” modulo ADC setup. The additional circuitry has minimal impact on the overall power consumption, and its penalty is fixed regardless of b . For instance, consider a flash ADC architecture for amplitude quantization. An 8-bit modulo ADC with no $c[n]$ would have $2^8 + 2 = 258$

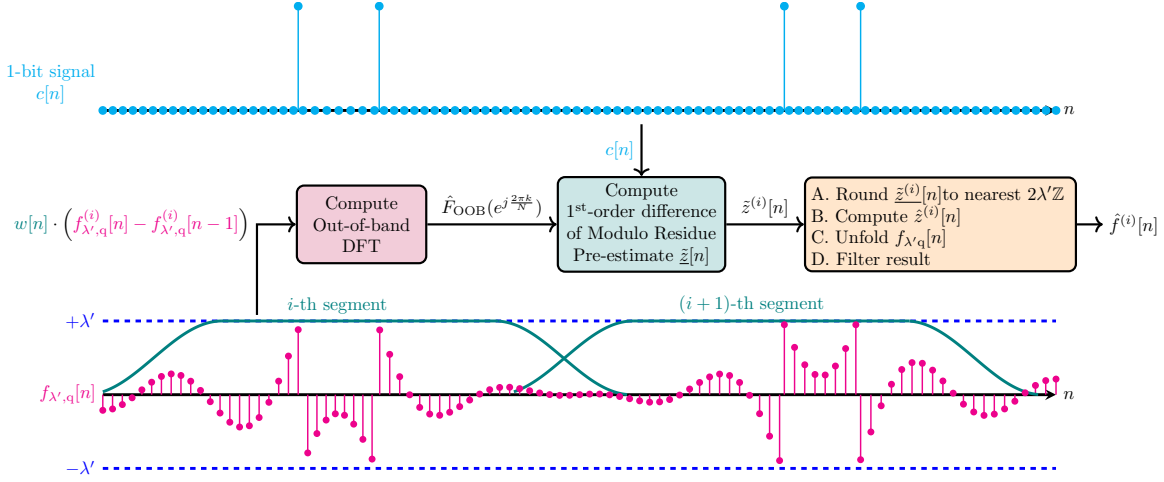


Fig. 3. Overview of the proposed sliding DFT-based unfolding method for modulo sampling.

comparators¹ whereas an 8-bit modulo ADC with 1-bit folding information $c[n]$ would have 259 comparators. The difference in comparator counts is fixed regardless of the number of bits for amplitude quantization. We also note that the folding information generated in Figure 1 is one bit less than the folding information generated by the modulo ADC hardware proposed in [32]. In [32], the 2-bit signal indicates three states: ‘no crossing’, ‘crossed $+\lambda'$ threshold’, ‘crossed $-\lambda'$ threshold’. Finally, we point out that the modulo ADC with 1-bit folding information has already been implemented in hardware [36], but it follows a different architecture from what is shown in Figures 1 and 2.

C. Signal Recovery Scheme

The proposed recovery algorithm first unfolds $f_{\lambda',q}[n]$ by estimating $z[n]$ and then reconstructs the continuous-time signal from the result. Since the sampling frequency used is above the Nyquist rate, the continuous-time signal can be uniquely identified using an appropriate reconstruction filter. In this subsection, we discuss the unfolding mechanism. An overview of the proposed unfolding procedure is given in Figure 3. The unfolding scheme multiplies a window signal $w[n]$ to small overlapping segments of $f_{\lambda',q}[n]$ and then recovers the modulo residue signal at each segment. The window is slid from left to right until the whole $f_{\lambda',q}[n]$ is processed.

Let N be the number of samples in a short segment of $f_{\lambda',q}[n]$. A length- N tapered cosine window $w[n]$ (a.k.a. Tukey window [51]) can be written as

$$w[n] = \begin{cases} \frac{1 + \cos\left(\frac{2\pi}{\alpha}\left(\frac{n}{N} - \frac{\alpha}{2}\right)\right)}{2}, & 0 \leq n < \frac{\alpha N}{2} \\ 1, & \frac{\alpha N}{2} \leq n < N\left(1 - \frac{\alpha}{2}\right) \\ \frac{1 + \cos\left(\frac{2\pi}{\alpha}\left(\frac{n}{N} - 1 + \frac{\alpha}{2}\right)\right)}{2}, & N\left(1 - \frac{\alpha}{2}\right) \leq n < N \end{cases},$$

where the parameter $\alpha > 0$ is the roll-off factor. We choose α so that $\alpha N \in 2\mathbb{Z}$.

¹The 2 additional comparators come from the comparators of the folding mechanism.

Suppose the i -th segment of $f_{\lambda',q}[n]$ is denoted as $f_{\lambda',q}^{(i)}[n]$ and the i -th segment of the unfolded signal as $f^{(i)}[n]$. Consecutive segments overlap such that the last $\frac{\alpha N}{2}$ samples of $f_{\lambda',q}^{(i-1)}[n]$ are the first $\frac{\alpha N}{2}$ samples $f_{\lambda',q}^{(i)}[n]$. The window function $w[n]$ is multiplied to the first-order difference of $f_{\lambda',q}[n]$ to get

$$\begin{aligned} \tilde{f}_w^{(i)}[n] &= w[n] \cdot f_{\lambda',q}^{(i)}[n] \\ &= w[n] \cdot \left(f_{\lambda',q}^{(i)}[n] - f_{\lambda',q}^{(i)}[n-1] \right), \end{aligned} \quad (3)$$

where $f_{\lambda',q}^{(i)}[-1] = f_{\lambda',q}^{(i-1)}[N-1] \forall i \in \{2, 3, \dots, I\}$ and we assume that $f_{\lambda',q}^{(1)}[-1] = 0$, i.e. signal starts at zero. We now describe the computation of the modulo residue samples in $f_{\lambda',q}^{(i)}[n]$. The principle behind the computation of the modulo residue samples is the Fourier domain separation between the bandlimited signal and the folding instances [10]. The length- N Discrete Fourier Transform (DFT) of $\tilde{f}_w^{(i)}[n]$ is computed as

$$\hat{F}_w(e^{j\frac{2\pi k}{N}}) = \frac{1}{\sqrt{N}} \sum_{n=0}^{N-1} \tilde{f}_w^{(i)}[n] e^{-j\frac{2\pi k n}{N}}. \quad (4)$$

Due to the finite bandwidth assumption on $f(t)$, $\hat{F}_w(e^{j\frac{2\pi k n}{N}})$ for $\frac{2\pi k}{N} \in (\rho\pi + \delta_{SL}, 2\pi - \rho\pi - \delta_{SL})$ can be written as

$$\begin{aligned} \hat{F}_{\text{OOB}}(e^{j\frac{2\pi k}{N}}) &= \frac{1}{\sqrt{N}} \sum_{n=0}^{N-1} w[n] \left[z^{(i)}[n] + \underline{\epsilon}^{(i)}[n] \right] e^{-j\frac{2\pi k n}{N}} \\ &= \frac{1}{\sqrt{N}} \sum_{n \in \mathcal{S}_i} w[n] \left[z_{\mathcal{S}_i}^{(i)}[n] + \underline{\epsilon}_{\mathcal{S}_i}^{(i)}[n] \right] e^{-j\frac{2\pi k n}{N}} \\ &\quad + \frac{1}{\sqrt{N}} \sum_{n \notin \mathcal{S}_i} w[n] \cdot \underline{\epsilon}_{\mathcal{S}_i}^{(i)}[n] \cdot e^{-j\frac{2\pi k n}{N}}, \end{aligned} \quad (5)$$

where the spectral leakage width, denoted δ_{SL} , accounts for the frequencies where spectral leakage is still significant. Some energy of the $\tilde{f}_w^{(i)}[n]$ may leak in the band $(\rho\pi, 2\pi - \rho\pi)$ due to the inherent spectral leakage in the DFT computation and cannot be neglected. Spectral leakage vanishes towards zero for high frequencies and cannot be made zero for any signal.

However, spectral leakage can be controlled by properly choosing the window length N and roll-off parameter α . The signals $\underline{z}^{(i)}[n]$ and $\underline{\epsilon}^{(i)}[n]$ are the first-order difference of the modulo residue samples and quantization noise, respectively, in $\tilde{f}_w^{(i)}[n]$. The set \mathcal{S}_i contains the indices for which $c[n] = 1$ in the i -th segment. The set identifies the indices in the i -th segment for which the DVG changes its output voltage. The samples $z_{\mathcal{S}_i}^{(i)}[n]$ (resp. $z_{\mathcal{S}_i^c}^{(i)}[n]$) corresponds to the value of the modulo residue for all n such that $c[n] = 1$ (resp. $c[n] = 0$) in the i -th segment. The subscript OOB in \hat{F}_{OOB} is used to indicate that this is the set of DFT coefficients outside the desired signal bandwidth plus non-negligible spectral leakage.

We are primarily interested in estimating $f^{(i)}[n]$. Our approach is to estimate $z^{(i)}[n]$ first and then subtract $z^{(i)}[n]$ from $f_{\lambda',q}^{(i)}[n]$. This procedure essentially unfolds the modulo ADC output. Let K be the number of discrete frequencies k such that $\frac{2\pi k}{N} \in (\rho\pi + \delta_{\text{SL}}, 2\pi - \rho\pi - \delta_{\text{SL}})$. Equation (5) can be written in matrix form as

$$\hat{\mathbf{F}}_{\text{OOB}} = \mathbf{V} (\mathbf{z}_w + \underline{\epsilon}_w), \quad (6)$$

where $\mathbf{z}_w \in \mathbb{R}^{N \times 1}$, $\underline{\epsilon}_w \in \mathbb{R}^{N \times 1}$, and $\hat{\mathbf{F}}_{\text{OOB}} \in \mathbb{C}^{K \times 1}$ are vectorized form of the finite-length signals $w[n] \cdot z^{(i)}[n]$, $w[n] \cdot \underline{\epsilon}^{(i)}[n]$, and $\hat{F}_{\text{OOB}}(e^{j\frac{2\pi k}{N}})$, respectively. The entry of matrix $\mathbf{V} \in \mathbb{C}^{K \times N}$ in the k' -th row and n -th column is $\frac{1}{\sqrt{N}} e^{-j\frac{2\pi n k}{N}}$, where $\frac{2\pi k}{N}$ is the k' -th discrete frequency in $(\rho\pi + \delta_{\text{SL}}, 2\pi - \rho\pi - \delta_{\text{SL}})$. Let $\mathbf{z}_{w,\mathcal{S}_i} \in \mathbb{R}^{|\mathcal{S}_i| \times 1}$ and $\underline{\epsilon}_{w,\mathcal{S}_i} \in \mathbb{R}^{|\mathcal{S}_i| \times 1}$ contain the elements of \mathbf{z}_w and $\underline{\epsilon}_w$ whose indices n are in \mathcal{S}_i . Then, a pre-estimate of $\mathbf{z}_{w,\mathcal{S}_i}$, denoted as $\tilde{\mathbf{z}}_{w,\mathcal{S}_i}$, can be expressed as

$$\tilde{\mathbf{z}}_{w,\mathcal{S}_i} = \mathbf{V}_{\mathcal{S}_i}^\dagger \hat{\mathbf{F}}_{\text{OOB}}, \quad (7)$$

where $\mathbf{V}_{\mathcal{S}_i} \in \mathbb{C}^{K \times |\mathcal{S}_i|}$ is formed by horizontally stacking the columns of \mathbf{V} whose column indices are in \mathcal{S}_i . We obtain the (windowed) pre-estimate of $z^{(i)}[n]$, denoted $\tilde{z}_w^{(i)}[n]$, by placing the corresponding values of $\tilde{\mathbf{z}}_{w,\mathcal{S}_i}$ to $\tilde{z}_w^{(i)}[n]$ for $n \in \mathcal{S}_i$. The values of $\tilde{z}_w^{(i)}[n]$ for $n \notin \mathcal{S}_i$ are set to 0.

Note that the n -th element of $\tilde{z}_w^{(i)}[n]$ for $n \in \{0, \dots, \frac{\alpha N}{2} - 1\}$ has a non-unity scaling of the desired modulo residue signal $z^{(i)}[n]$ due to the tapered cosine window $w[n]$. To correct this scaling, we exploit the symmetry of the window function at the edges:

$$w[n] + w[n + N(1 - \frac{\alpha}{2})] = 1 \quad \forall n \in \{0, 1, \dots, \frac{\alpha N}{2} - 1\}. \quad (8)$$

We take the last $\frac{\alpha N}{2}$ samples of $\tilde{z}_w^{(i-1)}[n]$ and add them to the first $\frac{\alpha N}{2}$ samples of $\tilde{z}_w^{(i)}[n]$ ². The resulting signal is

$$\tilde{z}_w^{(i)}[n] = \begin{cases} \tilde{z}_w^{(i)}[n] + \tilde{z}_w^{(i-1)}[n + N(1 - \frac{\alpha}{2})], & 0 \leq n < \frac{\alpha N}{2} \\ \tilde{z}_w^{(i)}[n], & \frac{\alpha N}{2} \leq n < N(1 - \frac{\alpha}{2}) \end{cases}$$

The scaling correction is illustrated in Figure 4. Since $z^{(i)}[n] \in 2\lambda'\mathbb{Z}$, $z^{(i)}[n] \in 2\lambda'\mathbb{Z}$. The samples of the first-order difference of modulo residue pre-estimates $\tilde{z}_w^{(i)}[n]$ are rounded to the nearest integer multiple of $2\lambda'$ to get the first-order difference

²Due to the sliding window approach, $\tilde{z}_w^{(i-1)}[n]$ is already available when processing the i -th segment of $f_{\lambda',q}^{(i)}[n]$

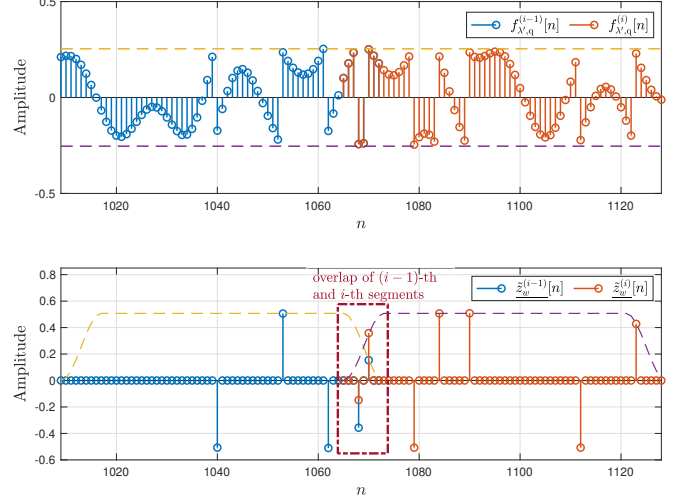


Fig. 4. Illustration of the scaling correction for $\tilde{z}_w^{(i)}[n]$. The top plot shows the folded samples of the modulo ADC for the $(i-1)$ -th and i -th segments, denoted $f_{\lambda',q}^{(i-1)}[n]$ (blue) and $f_{\lambda',q}^{(i)}[n]$ (red), respectively. The yellow and purple lines correspond to modulo thresholds. The bottom plot shows the first-order differences of the (windowed) modulo pre-estimates in the $(i-1)$ -th and i -th segments, denoted $\tilde{z}_w^{(i-1)}[n]$ (blue) and $\tilde{z}_w^{(i)}[n]$ (red), respectively. Due to the tapered cosine window, the recovered amplitudes of $\tilde{z}_w^{(i-1)}[n]$ and $\tilde{z}_w^{(i)}[n]$ in the overlap region (maroon box) are attenuated. However, adding the last $\alpha N/2$ samples of $\tilde{z}_w^{(i-1)}[n]$ to the first $\alpha N/2$ samples of $\tilde{z}_w^{(i)}[n]$ would correct the amplitude of $\tilde{z}_w^{(i)}[n]$ from $n \in \{0, \dots, \frac{\alpha N}{2} - 1\}$.

of the modulo residue estimates, denoted as $\hat{z}^{(i)}[n]$. To undo the first-order difference operation in the modulo residue signal, the formula

$$\hat{z}^{(i)}[n] = \hat{z}^{(i-1)}[n] + \hat{z}^{(i)}[n] \quad (9)$$

is applied. The modulo residue signal estimate $\hat{z}^{(i)}[n]$ is then subtracted from $f_{\lambda',q}^{(i)}[n]$ to unfold the i -th segment for $n \in \{0, \dots, N(1 - \frac{\alpha}{2})\}$. The recovery of the unfolded sequence continues until all segments of $f_{\lambda',q}^{(i)}[n]$ have been processed. If $c[n] = 0$ for all $n \in \{0, \dots, N-1\}$ in the i -th segment, we can skip the processing of i -th segment and proceed to the next one. Finally, a digital lowpass filter with passband region $(-\frac{\Omega_m}{2} - \delta_{\text{SL}}, +\frac{\Omega_m}{2} + \delta_{\text{SL}})$ is applied to the result, where $\Omega_m = \omega_m T_s$. The unfolded signal per segment can be expressed as

$$\hat{f}^{(i)}[n] = \left\{ f_{\lambda',q}^{(i)}[n] - \hat{z}^{(i)}[n] \right\}_{\text{LPF}} = f^{(i)}[n] + \left\{ z^{(i)}[n] - \hat{z}^{(i)}[n] \right\}_{\text{LPF}} + \epsilon_{\text{LPF}}^{(i)}[n]. \quad (10)$$

D. Proposed Recovery Scheme vs. Other DFT-based Techniques

Due to the DFT computation, our proposed recovery scheme can be classified as a DFT-based recovery technique. Other algorithms under this category are the Fourier-Prony method [10], USLSE [12], B^2R^2 [11], and LASSO- B^2R^2 [13]. The advantage of our proposed recovery scheme is that it does not restrict the signal to decay over time (such as in B^2R^2 and

LASSO- B^2R^2) nor does it require the signal to be periodic (such as in Fourier-Prony method). The window function ensures that sharp discontinuities are avoided at the periodic boundaries when the length- N sampled signal is repeated. Consequently, spectral leakage is minimized. The vanishing signal amplitude requirement in B^2R^2 and LASSO- B^2R^2 may require long observation time to estimate the modulo residue samples. The computational complexities of these algorithms grow fast with the observation length. In contrast, the proposed algorithm follows the principle of STFT and the observation length of a segment can be controlled. That is, we can either choose to unfold few overlapping segments with large observation length or many overlapping segments with small observation length. In addition, the sliding DFT approach enables processing of modulo samples in short frames. This is suitable for real-time applications with low latency requirement.

Our objective is to derive MSE performance guarantees for this recovery scheme and demonstrate the advantage of modulo ADCs which uses the proposed recovery scheme over conventional ADCs. In the next section, the main results of our paper are presented.

III. PERFORMANCE GUARANTEES USING THE PROPOSED RECOVERY PROCEDURE

A. Measuring Recovery Performance

Our primary measure of recovery performance of the unfolding scheme is the MSE between the (sampled) input signal $f[n]$ and the $\hat{f}[n]$, given by

$$\begin{aligned}
\text{MSE} &= \frac{1}{N_0} \sum_{n=0}^{N_0-1} \mathbb{E} \left\{ |\hat{f}[n] - f[n]|^2 \right\} \\
&= \frac{1}{NI} \sum_{i=1}^I \sum_{n=0}^{N-1} \mathbb{E} \left\{ |\hat{f}^{(i)}[n] - f^{(i)}[n]|^2 \right\} \\
&= \frac{1}{NI} \sum_{i=1}^I \sum_{n=0}^{N-1} \left| \left\{ z^{(i)}[n] - \hat{z}^{(i)}[n] \right\}_{\text{LPF}} \right|^2 \\
&\quad + 2\mathbb{E} \left\{ \epsilon_{\text{LPF}}^{(i)}[n] \right\} \left\{ z^{(i)}[n] - \hat{z}^{(i)}[n] \right\}_{\text{LPF}} \\
&\quad + \mathbb{E} \left\{ |\epsilon_{\text{LPF}}^{(i)}[n]|^2 \right\} \\
&= \frac{1}{NI} \sum_{i=1}^I \sum_{n=0}^{N-1} \left| \left\{ z^{(i)}[n] - \hat{z}^{(i)}[n] \right\}_{\text{LPF}} \right|^2 \\
&\quad + \mathbb{E} \left\{ |\epsilon_{\text{LPF}}^{(i)}[n]|^2 \right\}, \tag{11}
\end{aligned}$$

where N_0 is the signal length. The second line comes from partitioning the original signal into I length- N segments. The third line follows from the expression of the unfolded signal in equation (10) and from doing some algebraic manipulation. The fourth line comes from the fact that the quantization noise has zero mean. Thus, the second term in the third line can be removed.

From equation (11), it can be seen that the MSE expression comes from two sources: (1) the error due to the modulo residue estimation error and (2) the in-band quantization noise.

Our objective in this section is to derive the exact MSE expression as a function of OF and b when our proposed recovery procedure is used.

B. Statistical Model for Quantization Noise

Since MSE involves the mean square of the quantization noise, it is crucial to understand the statistical properties of the quantization noise. The statistical nature of the quantization noise comes from the dithered quantization framework established in [52]. This framework is appropriate for the modulo ADC since the folding operation ensures that the signal does not overload the quantizer. The ‘no overloading’ property of the modulo ADC, together with the triangle dither $d[n]$, guarantees that the quantization noise is a white process and its power does not depend on the input, i.e. $\mathbb{E} \{ |\epsilon[n]|^2 | f_{\mathcal{X}}[n] \} = \mathbb{E} \{ |\epsilon[n]|^2 \}$ (see [52, Theorem 2]). For triangle dither $d[n]$ described in Section II, the induced quantization noise has power $\mathbb{E} \{ |\epsilon[n]|^2 \} = \frac{1}{4} \left(\frac{2\lambda}{2^b} \right)^2 = \frac{\lambda^2}{2^{2b}}$.

C. Incorporating Spectral Leakage

Since spectral leakage cannot be completely neglected for small N , we explicitly account for the effect of non-negligible spectral leakage in the proposed recovery algorithm. To this end, we define the *spectral leakage bin count* as $K_{\text{SL}} = 2 \lceil \frac{\delta_{\text{SL}} N}{\pi} \rceil$, which corresponds to the number of discrete frequency bins within the spectral leakage intervals $(\rho\pi, \rho\pi + \delta_{\text{SL}}) \cup (2\pi - \rho\pi - \delta_{\text{SL}}, 2\pi - \rho\pi)$. While K_{SL} and δ_{SL} are generally difficult to compute exactly in practice due to their dependence on the precise shape of the leakage spectrum, we highlight their role in the MSE performance guarantee to reveal how spectral leakage affects recovery accuracy. Finally, we note that the MSE performance guarantee to be derived does not account for the spectral leakage inside $[\rho\pi + \delta_{\text{SL}}, 2\pi - \rho\pi - \delta_{\text{SL}}]$. Nonetheless, our numerical results in Section IV demonstrate that our theoretical MSE predictions still coincide with the simulated MSE despite neglecting some spectral leakage.

D. Main Result

Before we state the main result of this paper, a proposition about the matrix $\mathbf{V}_{\mathcal{S}_i}$ is first presented. This will play a key role in the derivation of the main result.

Proposition 1. *Let $f(t)$ be a bandlimited function. The matrices $\{\mathbf{V}_{\mathcal{S}_i}\}_i$ used in the recovery algorithm have full column rank if*

$$\text{OF} \geq \frac{N}{N - \max_i |\mathcal{S}_i| - K_{\text{SL}}}. \tag{12}$$

Proof. See Appendix A. \square

With $\mathbf{V}_{\mathcal{S}_i}$ being full column rank, $\mathbf{V}_{\mathcal{S}_i}^\dagger \mathbf{V}_{\mathcal{S}_i}$ is an $|\mathcal{S}_i| \times |\mathcal{S}_i|$ identity matrix. Under a ‘no quantization noise setting’, $\|\hat{\mathbf{z}}_{\mathcal{S}_i} - \mathbf{z}_{\mathcal{S}_i}\|_\infty = \|\mathbf{V}_{\mathcal{S}_i}^\dagger \mathbf{V}_{\mathcal{S}_i} \mathbf{z}_{\mathcal{S}_i} - \mathbf{z}_{\mathcal{S}_i}\|_\infty = 0$. Thus, the full column rank property is crucial for the recovery of $z^{(i)}[n]$.

One key observation to note in Proposition 1 is that the oversampling factor OF approaches to unity if $|\mathcal{S}_i|$ grows

strictly slower with N . This is true for finite-energy bandlimited functions due to their time-domain decay property (see [11], [13]). That is, $\exists n_0$ such that $f[n] < \lambda'$ for all $|n| > n_0$. Consequently, $\exists N_0$ such that $|\mathcal{S}_i|$ does not change $\forall N > N_0$. Thus, the sampling rate can be made closer to the Nyquist rate for finite-energy bandlimited signals at the expense of longer observation window. Similar trend is observed in the recovery guarantees established in [15]. That is, for signals that are compact λ -exceedance with parameter ρ_e , smaller OF can be used by increasing the number of observations. This λ -exceedance property is closely related to the time-domain decay property in [11], [13].

The drawback of Proposition 1 is that it depends on the bandlimited input signal $f(t)$. The following proposition provides a sufficient condition for OF that depends only on the maximum amplitude $\|f(t)\|_\infty$ and not on the whole $f(t)$.

Proposition 2. *The matrices $\{\mathbf{V}_{\mathcal{S}_i}\}_i$ used in the recovery algorithm have full column rank if*

$$\text{OF} \geq \frac{3}{1 - \frac{K_{\text{SL}}}{N}}. \quad (13)$$

This is achieved by setting the modulo threshold to

$$\lambda' = \frac{\|f(t)\|_\infty}{\text{OF} \cdot \left[1 - \frac{K_{\text{SL}}}{N}\right] - 2}. \quad (14)$$

Proof. See Appendix B. \square

Note that Proposition 2 is a sufficient but not a necessary condition. The expression we used to bound $\max_i |\mathcal{S}_i|$ from above is identical to the bound of the folding instances derived in [13, Equation 8]. However, their proof assumed that $f(t)$ is a bandlimited signal with negligible truncation error. We show in Appendix B that this bound is also valid for the setup considered in this paper. However, this bound can be loose in some cases as demonstrated in [13, Table 1].

For N approaching infinity, equation (13) simplifies to $\text{OF} > 3$, which was derived in [14]. The theoretical MSE guarantee established in [14] did not take into account the spectral leakage. As demonstrated in Proposition 2, the spectral leakage bin count K_{SL} increases the required OF to satisfy condition (13). Nonetheless, its effect on the OF sufficient condition diminishes fast as N grows.

We can now state the main theoretical result of this paper. The following theorem establishes the MSE of the proposed recovery method when the parameters OF and b are above certain values.

Theorem 1. *Suppose*

$$\text{OF} \geq \frac{3}{1 - \frac{K_{\text{SL}}}{N}} \quad (15)$$

and

$$b > 3 + \log_2 \left(1 + \frac{3M}{4}\right), \quad (16)$$

where $M = \max_i \|\mathbf{V}_{\mathcal{S}_i}^\dagger \mathbf{V}_{\mathcal{S}_i}\|_\infty$. The MSE incurred by the proposed recovery algorithm can be written as

$$\text{MSE} = \frac{\|f(t)\|_\infty^2 \left(1 + \frac{\delta_{\text{SL}}}{\pi} \cdot \text{OF}\right)}{\text{OF} \cdot (2^b - 2)^2 \cdot \left(\text{OF} \left[1 - \frac{K_{\text{SL}}}{N}\right] - 2\right)^2}. \quad (17)$$

This is achieved by setting the modulo threshold to

$$\lambda' = \frac{\|f(t)\|_\infty}{\text{OF} \cdot \left[1 - \frac{K_{\text{SL}}}{N}\right] - 2}. \quad (18)$$

Proof. See Appendix C. \square

The intuition behind the result is that the range of OF and b in Theorem 1 guarantees that the bounded noise added to the modulo residue pre-estimate $\hat{z}^{(i)}[n]$ is within $(-\lambda', +\lambda')$. Since $\hat{z}^{(i)}[n]$ are integer multiples of $2\lambda'$, the rounding operation maps all modulo residue pre-estimates $\hat{z}^{(i)}[n]$ to the correct modulo residue $z^{(i)}[n]$. Consequently, only the quantization noise power term in equation (11) appears in the MSE expression.

The derivation of [14, Theorem 1] did not take into account the contribution of the $\epsilon^{(i)}[n]$ for $n \in \mathcal{S}_i^c$, resulting in $b > 3$ condition. In our Theorem 1, the second term in equation (16) accounts for the impact of $\epsilon_{\mathcal{S}_i^c}^{(i)}[n]$ on the recovery performance. Although we are interested in the modulo residue samples located at \mathcal{S}_i , $\epsilon_{\mathcal{S}_i^c}^{(i)}[n]$ still contributes to $\hat{z}^{(i)}[n]$ through the computation of $\hat{F}_{\text{OoB}}(e^{j\frac{2\pi k}{N}})$. In Section IV, we investigate how the second term of (16) is affected by parameters such as segment length, cardinality of \mathcal{S}_i , and oversampling factor.

It is also important to point out the detrimental impact of spectral leakage to the MSE performance. Neglecting spectral leakage, i.e. $\delta_{\text{SL}} = 0$, equation (17) simplifies to

$$\begin{aligned} \text{MSE} &= \frac{\|f(t)\|_\infty^2}{\text{OF} \cdot (2^b - 2)^2 \cdot (\text{OF} - 2)^2} \\ &= \mathcal{O}\left(\frac{1}{\text{OF}^3}\right) \end{aligned} \quad (19)$$

This is similar to the asymptotic growth rate established in [14] which neglected spectral leakage. When $\delta_{\text{SL}} > 0$, the asymptotic growth rate of the MSE becomes $\mathcal{O}\left(\frac{1}{\text{OF}^2}\right)$ only. δ_{SL} can be reduced if larger window length is used. However, using a larger window length increases the computational complexity of the sliding window DFT (see Section III-G).

E. Comparison with Recovery Guarantees of Existing Methods

We now compare the derived theoretical results with other performance guarantees derived for modulo sampling. One popular recovery procedure is the higher-order differences (HoD) approach developed in [7]. Performance guarantee for this algorithm under a bounded noise setting (e.g., quantization noise) has been analyzed in [7, Theorem 6]. More precisely, they showed that for finite-energy bandlimited signals, the noisy unfolded samples can be recovered from noisy modulo samples up to an unknown additive constant, i.e.,

$$\hat{f}_{\text{HoD}}[n] = f[n] + \epsilon[n] + 2\lambda'p,$$

where $p \in \mathbb{Z}$ is not known, if the sampling rate is at least $2^\alpha \pi e \times f_{\text{Nyq}}$. Here, $\alpha \in \mathbb{N}$ is a parameter of the bounded noise and depends on both the maximum amplitude of the noise and the modulo threshold. In contrast, Theorem 1 only requires $\text{OF} > 3$ under negligible spectral leakage. We also note that $\text{OF} > 3$ closely resembles the OF requirement derived in

[53] to uniquely identify periodic bandlimited signals under the modulo-DFT sensing model. However, their model first applies DFT on the sampled signal prior to modulo operation. Moreover, the $\text{OF} > 3$ result is equivalent to Itoh's condition [54] and is reminiscent of the spatial oversampling requirement established for DoA estimation using MIMO arrays with modulo nonlinearities [33].

A prediction-based approach [16] showed that OF can be made arbitrarily close to unity in exchange for a significant increase in prediction filter length. However, it was pointed out in [16, Section III] that their proposed approach “*collapses in the presence of quantization noise*”. In contrast, our algorithm can work with finite quantization bits. Moreover, our proposed algorithm can work at a sampling rate arbitrarily close to the Nyquist rate for finite-energy bandlimited signals and sufficiently large window length N by virtue of Proposition 1. We also note that the OF requirement established in [10] for periodic bandlimited signals is

$$\text{OF} \geq \frac{N}{N - 2|\mathcal{S}| - 2},$$

where $|\mathcal{S}|$ is the number of folding instances. Evidently, when $K_{\text{SL}} = 0$, the sufficient condition on OF established in Proposition 1 is better than the OF requirement in [10]. The advantage of Proposition 1 might be attributed to the availability of the 1-bit folding information in our setup.

Finally, there exists a line of work [28], [29], [31] which uses time-domain thresholding to unfold the output produced by generalized modulo sampling models. Unlike the DFT-based recovery methods, thresholding is done in the time domain so spectral leakage is not an issue. Moreover, thresholding-based techniques have established recovery guarantees [28], [29]. However, the sequential estimation of the folding parameters requires that the folding times are well-separated in the time domain. Such separation cannot be guaranteed under ideal modulo sampling with zero hysteresis as demonstrated in [29, Lemma 1]. Moreover, the MSE bound established in [29, Proposition 1] is inversely proportional to the hysteresis h . Under ideal modulo nonlinearities, this h goes to zero and so the MSE under the thresholding-based recovery becomes unbounded.

F. Comparison with Conventional ADCs

To demonstrate the advantage of a modulo ADC with 1-bit folding side information over a conventional ADC, we first derive the MSE of a conventional b -bit ADC under the non-subtractive dithered quantization framework. We compare the modulo ADC and conventional ADC under the same bit budget used for amplitude quantization. For a triangle dither $d[n] \in (-\frac{2\lambda}{2^b}, +\frac{2\lambda}{2^b})$, the ADC parameter λ should be set to $\lambda = (1 + \frac{1}{2^b}) \|f(t)\|_\infty$. After digital filtering, the quantization noise power (which is also the MSE) becomes

$$\text{MSE}_{\text{conv}} = \frac{\|f(t)\|_\infty^2}{\text{OF}(2^b - 2)^2}. \quad (20)$$

Comparing the MSE guarantee for modulo ADC in Theorem 1 and the derived MSE for a conventional ADC, it can be observed that $\text{MSE}_{\text{mod}} = \mathcal{O}(\frac{1}{\text{OF}^2})$ while $\text{MSE}_{\text{conv}} = \mathcal{O}(\frac{1}{\text{OF}})$

under sufficiently large b . The fast decay rate of MSE_{mod} with respect to OF is due to the reduction of the ADC parameter λ . Smaller ADC range entails smaller quantization bins. This demonstrates the superior performance of modulo ADCs over conventional ADCs in oversampled systems. Still, the modulo ADC has a slightly higher hardware complexity due to the folding operation and the 1-bit side information $c[n]$.

G. Computational Complexity

We now derive the computational complexity of the proposed algorithm in terms of the signal length N_0 , window length N , window roll-off α ($0 \leq \alpha \leq 1$) and oversampling factor $\text{OF} = \frac{1}{\rho}$. The number of segments depends on the ratio $\frac{N_0}{N}$, and the parameter α dictates how large is the overlap between consecutive segments. For large N_0 , the number of segments to be processed by the algorithm is in $\mathcal{O}(\frac{N_0}{N(1-\alpha/2)})$. Looking at the complexity of the residual recovery algorithm at each frame, the calculation of $\mathbf{V}_{\mathcal{S}_i}^\dagger \in \mathbb{C}^{|\mathcal{S}_i| \times K}$ is the most computationally-expensive operation. More precisely, this calculation is in $\mathcal{O}(K|\mathcal{S}_{\text{max}}|^2)$, where $|\mathcal{S}_{\text{max}}| = \max_i |\mathcal{S}_i|$. Since $K \approx (1 - \rho)N$ and $|\mathcal{S}_{\text{max}}| \leq K$ under appropriate choice of OF and λ' , then the complexity of computing $\mathbf{V}_{\mathcal{S}_i}^\dagger$ is in $\mathcal{O}((1 - \rho)^3 N^3)$. Considering all the segments to be processed, the overall computational complexity of the proposed recovery method is in $\mathcal{O}(\frac{N_0(1-\rho)^3 N^2}{1-\alpha/2})$. Hence, the computational complexity of our proposed algorithm is linear in the signal length N_0 .

Based on the derived computational complexity of the proposed algorithm, the speed of the proposed sliding DFT-based recovery scheme can be improved by choosing a small oversampling factor (high ρ) that satisfies the sufficient condition in Theorem 1. However, reducing OF negatively impacts the MSE as shown in equation (17). The speed of the proposed sliding DFT-based recovery scheme can also be improved by choosing a small window length N . However, a small window length also needs a higher α to compensate for the increased spectral leakage. Finally, we note that the recovery algorithm in [14], [48] is a special case of our proposed recovery algorithm with $N = N_0$ and $\alpha = 0$, i.e., rectangular window with no overlap. Hence, its complexity is in $\mathcal{O}((1 - \rho)^3 N_0^3)$. Since N is typically chosen to be much smaller than N_0 , our proposed sliding DFT-based recovery is $\mathcal{O}(\frac{N_0^2(1-\alpha/2)}{N^2})$ faster than the recovery algorithm in [14]. Suppose the signal to be processed has $N_0 = 100,000$ samples. Our proposed algorithm with sliding window length $N = 256$ and roll-off parameter $\alpha = 0.25$ can unfold the whole signal at roughly 7.48×10^{-6} times the total time needed by the recovery method in [14], [48] to unfold the whole signal.

IV. NUMERICAL RESULTS

In this section, we validate the MSE performance guarantees for the proposed algorithm established in the previous section by comparing the theoretical MSE results with the simulated performance. Numerical experiments are also conducted to gain additional insight on how the algorithm parameters affect the performance guarantees. We also compare the proposed sliding DFT recovery against the HoD-based recovery.

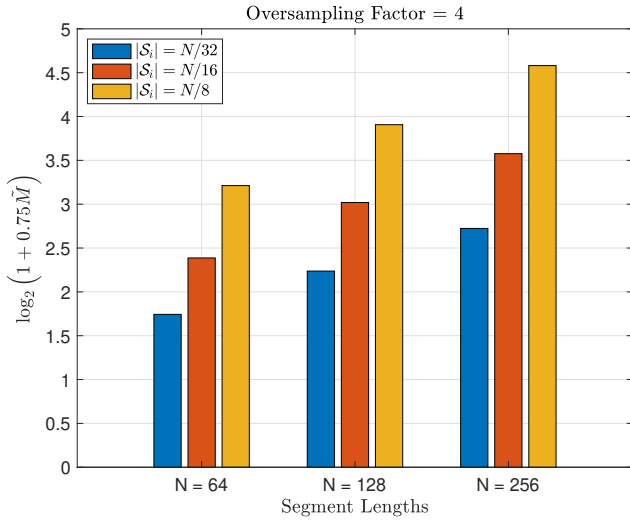


Fig. 5. Empirical evaluation of $\log_2(1 + 0.75\tilde{M})$ as a function of segment length (N) and $|\mathcal{S}_i|$ for OF = 4.

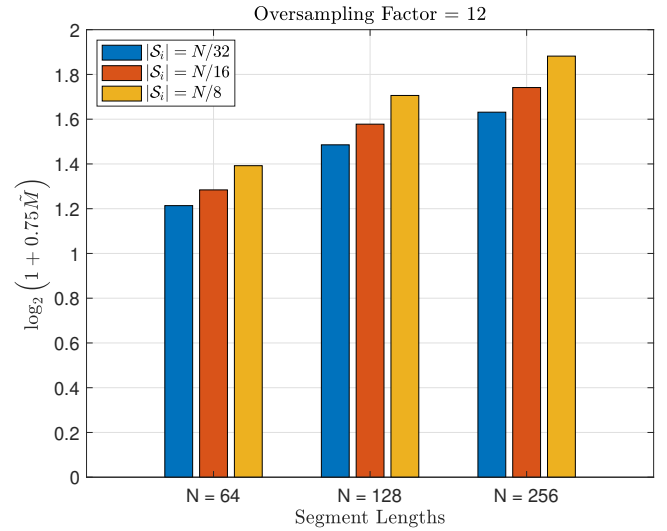


Fig. 7. Empirical evaluation of $\log_2(1 + 0.75\tilde{M})$ as a function of segment length (N) and $|\mathcal{S}_i|$ for OF = 12.

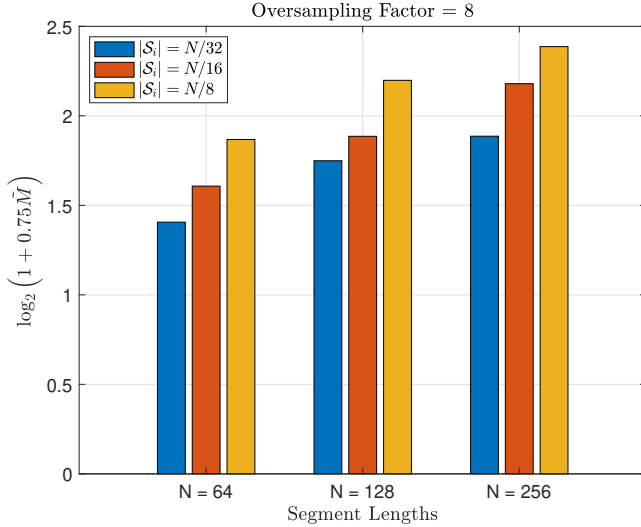


Fig. 6. Empirical evaluation of $\log_2(1 + 0.75\tilde{M})$ as a function of segment length (N) and $|\mathcal{S}_i|$ for OF = 8.

A. Analysis of the Sufficient Condition for b

We first investigate how the sufficient condition on b (i.e., equation (16)) is affected by algorithm and input signal parameters such as segment length N , oversampling factor OF, and number of non-zero elements of the 1-bit folding information signal $c[n]$. To this end, we consider three OF parameter settings (OF = 4, 8, 12) and three segment lengths ($N = 64, 128, 256$). We also consider three values of $|\mathcal{S}_i|$ ($|\mathcal{S}_i| = \frac{N}{32}, \frac{N}{16}, \frac{N}{8}$). For each combination of these parameter settings, we generate 100,000 realizations of $\mathbf{V}_{\mathcal{S}_i}$ by selecting $|\mathcal{S}_i|$ out of N columns of \mathbf{V} . We then estimate the second term of equation (16) by calculating

$$\tilde{M} = \max_{i \in \{1, 2, \dots, 100,000\}} \|\mathbf{V}_{\mathcal{S}_i}^\dagger \mathbf{V}_{\mathcal{S}_i^c}\|_\infty, \quad (21)$$

where the index i iterates over all 100,000 random realizations of $\mathbf{V}_{\mathcal{S}_i}$.

Figures 5-7 depict the empirical evaluation of $\log_2(1 + 0.75\tilde{M})$ for OF = 4, OF = 8, and OF = 12, respectively. This term accounts for the extra bit resolution needed by the proposed algorithm (in addition to the 3 bits in the first term of equation (16)) to satisfy the sufficient condition. Based on these evaluations, it can be seen that using a higher oversampling factor generally decreases the second term of equation (16). One insight that can be drawn from this observation is that a reduction in the modulo ADC resolution can be compensated by oversampling. Figures 5-7 also show that longer segment length and frequent crossing of the modulo thresholds increase \tilde{M} .

As a final note in this numerical experiment, the sufficient condition for b derived in the previous section may not be tight. We show in the succeeding numerical experiment that the proposed algorithm can achieve the performance guarantees in Theorem 1 even if we set $b = 4$.

B. Theoretical vs. Simulated MSE of the Sliding DFT-based Unfolding

To demonstrate the validity of the theoretical MSE guarantees, we consider the input signal

$$f(t) = \sum_{m=1}^{50,000} A_m \cdot p_{rc}(t - mT), \quad (22)$$

where $p_{rc}(t)$ is a raised-cosine pulse with roll-off parameter $\beta = 1$. For the numerical simulation, we set the filter span of the raised-cosine pulse to 20. The peak amplitude of the raised-cosine pulse $p_{rc}(t)$ is set to unity. The pulse amplitude A_m is drawn uniformly from the interval $[-0.5, +1]$, and $T = 1$ second is the time difference between two consecutive pulses. Intuitively, the signal $f(t)$ is constructed by generating 50,000 raised-cosine pulses with random amplitudes at every

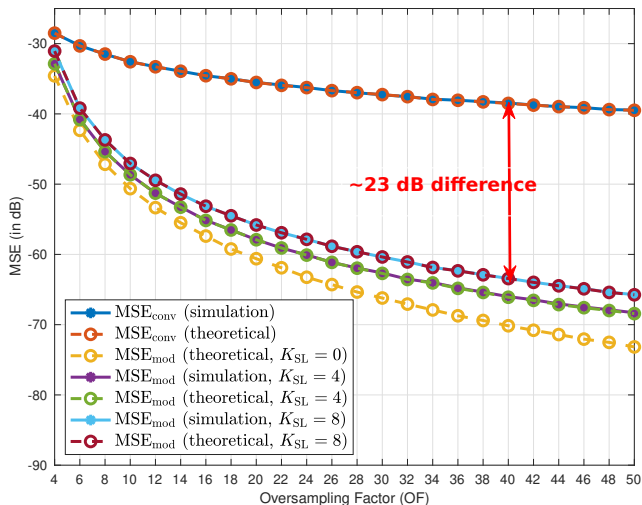


Fig. 8. Simulated and theoretical MSE vs. oversampling factor of the proposed sliding DFT-based unfolding algorithm for $N = 64$, $\alpha = 0.5$, $b = 4$ and $K_{SL} = 4, 8$. Superimposed in the figure are the simulated and theoretical MSE curves of a conventional ADC

symbol period T . Consequently, the maximum frequency is $\frac{\omega_m}{2} = \frac{\pi(1+\beta)}{T}$. The interval is chosen so that $f(t)$ has a non-zero mean value. We want to show that the algorithm can work on signals with non-zero average value. This signal is fed to a low-resolution 4-bit modulo ADC with sampling rate $\frac{1}{T_s} = \frac{OF\omega_m}{2\pi}$ to produce the quantized modulo samples $f_{\lambda',q}[n]$. The dither sequence and modulo threshold are configured according to the modulo ADC parameters.

For the sliding DFT-based recovery algorithm, we set the roll-off parameter of the tapered cosine window to $\alpha = 0.5$ and window length $N = 64$. Note that the length of the tapered cosine window is also the segment length and the DFT size of the algorithm. To investigate the impact of spectral leakage, we consider two different spectral leakage values: $\delta_{SL} = \frac{\pi}{32}$, $\frac{\pi}{16}$ (resp. $K_{SL} = 4, 8$). The spectral leakage in the discrete frequency interval $(\rho\pi + \delta_{SL}, 2\pi - \rho\pi - \delta_{SL})$ is assumed to be negligible. We will show later that this assumption is indeed valid for this simulation setup since the theoretical and simulated MSE performances coincide. Equation (18) is used to specify the modulo threshold λ' . The simulated performance is evaluated by taking the squared difference between the true samples $f[n]$ and the signal unfolding output $\hat{f}[n]$ and averaging the results over all N_0 samples.

Figure 8 depicts the simulated MSE (in decibels) of the modulo ADC with sliding DFT recovery and its theoretical MSE (based on Theorem 1) under the aforementioned settings. The oversampling factor is swept from $OF = 4$ to $OF = 50$. The numerical results for modulo ADC demonstrate that the derived MSE performance guarantee is accurate since it coincides with the simulated MSE for all OF and K_{SL} settings considered. It can be observed that larger δ_{SL} increases the MSE of the sliding DFT unfolding method. This can be attributed to two things: (a) the widening of the passband region of the digital LPF used in the last step of the unfolding

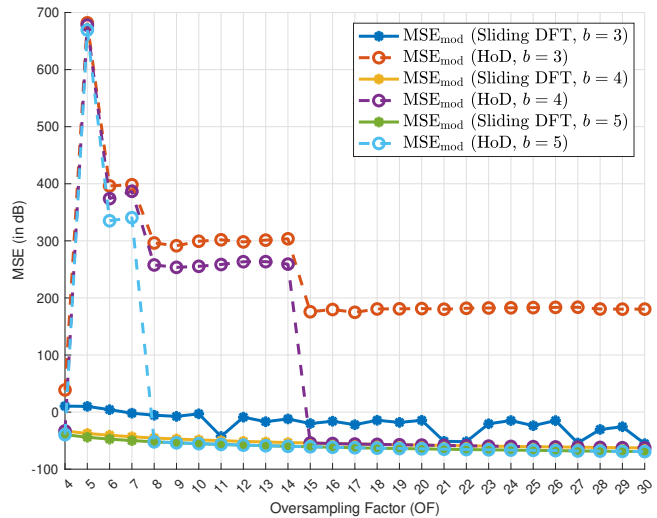


Fig. 9. Simulated MSE vs. oversampling factor of the sliding DFT-based recovery and HoD-based recovery for $b = 3, 4, 5$.

method, and (b) the increase in the λ' . Consequently, higher quantization noise power would be present at the digital LPF output.

The theoretical MSE curve for $K_{SL} = 0$ (i.e. spectral leakage neglected) is also superimposed in Figure 8. It is evident from the figure that the slope of the $K_{SL} = 0$ MSE curve is steeper at the high OF regime compared to those of $K_{SL} = 4$ and $K_{SL} = 8$ MSE curves. This validates the asymptotic MSE growth rates mentioned in Section III. Nonetheless, the modulo ADC which uses our sliding DFT recovery still outperforms the conventional ones even if there is spectral leakage. The gap between the MSE curves of the modulo ADC and conventional ADC widens as OF is increased. At $OF = 40$, the difference between the MSE incurred by the conventional ADC and the MSE incurred by the proposed sliding DFT-based recovery with $K_{SL} = 8$ is roughly 23 dB.

C. Comparison between the Sliding DFT-based recovery and HoD-based recovery

We now compare the performance of the proposed sliding DFT recovery against an existing unfolding method for modulo sampling. Note that it is not practical to unfold $f(t)$ in (22) using the DFT-based methods described in [10], [11], [13], [14], [36], [48] due to its large N_0 and its lack of periodicity. Moreover, the thresholding-based recovery method in [28, Algorithm 1] is unsuitable for the given $f(t)$, as it requires a minimum separation between folding times to function correctly. The low-sampling-rate variant [28, Algorithm 2] is likewise impractical due to its $\mathcal{O}(N_0^2)$ computational complexity. As a benchmark, we compare our proposed sliding DFT-based recovery method against the HoD modulo recovery approach [6], [7].

Figure 9 shows the simulated MSE performance of the proposed sliding DFT-based recovery method compared to the HoD-based recovery for different values of OF and b . The

parameters for the sliding DFT-based method are the same as in Section IV-B, except with $\delta_{\text{SL}} = \frac{\pi}{32}$. For both methods, the modulo threshold λ' is set according to (18) and the test signal $f(t)$ is given in (22). When $b = 4$ or $b = 5$, the proposed method successfully unfolds the modulo ADC output across all OF values considered. In contrast, the HoD-based recovery shows very high MSE for $4 < \text{OF} < 15$ when $b = 4$, and for $4 < \text{OF} < 8$ when $b = 5$. These results highlight the advantage of the proposed sliding DFT-based recovery over HoD-based recovery in the low-sampling-rate, low-resolution regime. The performance advantage of our proposed sliding DFT-based recovery over HoD could be attributed to the availability of the 1-bit folding information.

We also note that both methods fail to unfold the modulo ADC output when $b = 3$, suggesting that $b > 3$ may be a necessary condition for the successful operation of the sliding DFT-based recovery in its current form. Further research is needed to confirm this conjecture. Alternatively, employing other quantizer architectures in conjunction with modulo sampling may enable sliding DFT-based unfolding at resolutions below $b = 4$. For instance, the one-bit unlimited sampling approach in [55] uses a 1-bit sigma-delta quantizer together with modulo sampling to implement a 1-bit modulo ADC.

V. SUMMARY AND FUTURE DIRECTIONS

In this work, we considered a modulo ADC system in which the output samples are associated with a 1-bit folding information signal $c[n]$. The unfolded samples are obtained using the sliding DFT-based recovery scheme described in Section II-C. The advantage of our proposed unfolding scheme over existing Fourier-based recovery algorithms for modulo sampling is the significant reduction in the length of the observation window. This reduction in the observation time has a positive impact in the algorithm's computational complexity. We also provide sufficient conditions on the oversampling factor and ADC resolution to attain a certain MSE performance guarantee. When these sufficient conditions are met, the MSE performance of the modulo ADC which uses our proposed recovery method is better compared to that of conventional ADCs. Moreover, we also showed that spectral leakage affects the asymptotic MSE growth rate of our sliding DFT recovery method. These theoretical results are substantiated by the numerical experiments conducted in Section IV. Under the same modulo threshold setting and $b = 4, 5$, the proposed sliding DFT recovery method also outperformed the HoD-based recovery at low values of the oversampling factor.

It is worth mentioning that while the proposed unfolding scheme relies on the availability of 1-bit folding information signal $c[n]$, the proposed recovery can be modified to work without $c[n]$. This can be done by performing robust sparse recovery of $\tilde{z}_w^{(i)}[n]$ using a sliding DFT version of the LASSO- B^2R^2 [13] or a sliding DFT version of the OMP-based unfolding in [48]. This idea, together with its performance guarantees, is considered a potential subject of future work. We also note that the sufficient conditions derived for the oversampling factor and ADC resolution are not tight. Hence, another future direction is to tighten these sufficient conditions.

The modulo sampling architecture considered in this work did not take into account non-ideal modulo nonlinearities such as hysteresis and folding transients. Thus, we also intend to apply the sliding DFT recovery to generalized modulo sampling models and analyze how modulo hysteresis and folding transients affect the algorithm's performance. Lastly, it is also of interest to apply this proposed recovery algorithm to specific low-resolution signal processing systems (e.g., communication receivers, radars, etc.).

APPENDIX A

PROOF OF PROPOSITION 1

A necessary condition for $\mathbf{V}_{\mathcal{S}_i}$ to be full column rank is $|\mathcal{S}_i| \leq K$. Since the columns of $\mathbf{V}_{\mathcal{S}_i}$ are derived from the columns of the Fourier basis, they are linearly independent. Thus, the condition $|\mathcal{S}_i| \leq K$ is also sufficient. The number of discrete frequencies in the out-of-band region can be lower bounded by

$$K \geq N(1 - \rho) - K_{\text{SL}}. \quad (23)$$

To establish $|\mathcal{S}_i| \leq K$, it suffices to show that

$$|\mathcal{S}_i| \leq N(1 - \rho) - K_{\text{SL}}$$

or, equivalently,

$$\text{OF} \geq \frac{N}{N - |\mathcal{S}_i| - K_{\text{SL}}}. \quad (24)$$

for all i . Here, we used $\text{OF} = \frac{1}{\rho}$. The proof is completed by taking the maximum over all $|\mathcal{S}_i|$.

APPENDIX B

PROOF OF PROPOSITION 2

We first bound the size of \mathcal{S}_i using an expression that is independent of the segment index. To do this, we note that a real bandlimited signal $f(t)$ crosses a fixed level ℓ in a time interval of length T at most $2f_B T$ times, where f_B is the bandwidth of $f(t)$. Consider the time interval that corresponds to the i -th segment. Since $2f_B = \frac{\omega_m}{2\pi}$ and $T = NT_s = \frac{2\pi N}{\text{OF} \cdot \omega_{\text{sp}}}$, the number of times that $f(t)$ crosses level ℓ is at most $\frac{N}{\text{OF}}$. Moreover, the number of $(2\mathbb{Z} + 1)\lambda'$ folding levels in $f(t)$ is $2 + 2\lfloor \frac{\|f(t)\|_\infty - \lambda'}{2\lambda'} \rfloor$ as shown in [13]. Consequently, $|\mathcal{S}_i|$ is bounded as follows:

$$\begin{aligned} |\mathcal{S}_i| &\leq \frac{N}{\text{OF}} \left(2 + 2 \left\lfloor \frac{\|f(t)\|_\infty - \lambda'}{2\lambda'} \right\rfloor \right) \\ &\leq \frac{N}{\text{OF}} \left(1 + \frac{\|f(t)\|_\infty}{\lambda'} \right) \end{aligned} \quad (25)$$

for all i . The first line follows from multiplying the number of level crossings in a single level and the number of folding levels. The second line comes from the trivial lower bound of the floor function, i.e., $\lfloor x \rfloor \leq x$. Since the bound in equation (25) is independent of i , this bound is also an upper bound for $\max_i |\mathcal{S}_i|$. Using equation (25), the following inequality holds:

$$\frac{N}{N - \frac{N}{\text{OF}} \left(1 + \frac{\|f(t)\|_\infty}{\lambda'} \right) - K_{\text{SL}}} \geq \frac{N}{N - \max_i |\mathcal{S}_i| - K_{\text{SL}}}. \quad (26)$$

Consequently, setting

$$\text{OF} \geq \frac{N}{N - \frac{N}{\text{OF}} \left(1 + \frac{\|f(t)\|_\infty}{\lambda'}\right) - K_{\text{SL}}}$$

ensures that Proposition 1 is satisfied by transitivity. We can isolate OF on one side to get

$$\text{OF} \geq \frac{\frac{\|f(t)\|_\infty}{\lambda'} + 2}{1 - \frac{K_{\text{SL}}}{N}}. \quad (27)$$

Using

$$\lambda' = \frac{\|f(t)\|_\infty}{\text{OF} \cdot \left[1 - \frac{K_{\text{SL}}}{N}\right] - 2}$$

as the modulo threshold satisfies the inequality in (27). However, since $\lambda' \leq \|f(t)\|_\infty$, then

$$\text{OF} \cdot \left[1 - \frac{K_{\text{SL}}}{N}\right] - 2 \geq 1.$$

This implies that $\text{OF} \geq \frac{3}{1 - \frac{K_{\text{SL}}}{N}}$ must also hold. The OF requirements are satisfied simultaneously if equation (13) holds.

APPENDIX C PROOF OF THEOREM 1

As an initial step, an ℓ_∞ -norm bound on the difference between the modulo residue pre-estimate $\tilde{\mathbf{z}}$ and modulo residue \mathbf{z} is established:

$$\begin{aligned} \|\tilde{\mathbf{z}} - \mathbf{z}\|_\infty &= \|\tilde{\mathbf{z}}_{\mathcal{S}_i} - \mathbf{z}_{\mathcal{S}_i}\|_\infty \\ &= \|\mathbf{V}_{\mathcal{S}_i}^\dagger \hat{\mathbf{F}}_{\text{OOB}} - \mathbf{z}_{\mathcal{S}_i}\|_\infty \\ &= \|\mathbf{V}_{\mathcal{S}_i}^\dagger \mathbf{V}_{\mathcal{S}_i} (\mathbf{z}_{\mathcal{S}_i} + \underline{\boldsymbol{\epsilon}}_{\mathcal{S}_i}) + \mathbf{V}_{\mathcal{S}_i}^\dagger \mathbf{V}_{\mathcal{S}_i^c} \underline{\boldsymbol{\epsilon}}_{\mathcal{S}_i^c} - \mathbf{z}_{\mathcal{S}_i}\|_\infty \\ &= \|\mathbf{V}_{\mathcal{S}_i}^\dagger \mathbf{V} \underline{\boldsymbol{\epsilon}}\|_\infty \\ &\leq \left(1 + \|\mathbf{V}_{\mathcal{S}_i}^\dagger \mathbf{V}_{\mathcal{S}_i^c}\|_\infty\right) \cdot \|\underline{\boldsymbol{\epsilon}}\|_\infty \\ &\leq \left(1 + \|\mathbf{V}_{\mathcal{S}_i}^\dagger \mathbf{V}_{\mathcal{S}_i^c}\|_\infty\right) \cdot \left(\frac{6\lambda}{2^b}\right) \\ &= \left(1 + \|\mathbf{V}_{\mathcal{S}_i}^\dagger \mathbf{V}_{\mathcal{S}_i^c}\|_\infty\right) \cdot \left(\frac{6\lambda'}{2^b - 2}\right). \end{aligned}$$

The first line comes from the fact that $\tilde{z}^{(i)}[n] = z^{(i)}[n] = 0$ for $n \notin \mathcal{S}_i$. The second and third lines come from equations (6) and (7). Because the last $\frac{\alpha N}{2}$ samples of $\tilde{z}_w^{(i-1)}[n]$ is added to the first $\frac{\alpha N}{2}$ samples of $\tilde{z}_w^{(i)}[n]$, the effect of the window function is removed. Consequently, the subscript w is dropped in the second line. The fourth line holds because $\mathbf{V}_{\mathcal{S}_i}$ is full column rank by Proposition 2 and $\mathbf{V}_{\mathcal{S}_i}^\dagger \mathbf{V}_{\mathcal{S}_i} \underline{\boldsymbol{\epsilon}}_{\mathcal{S}_i} + \mathbf{V}_{\mathcal{S}_i}^\dagger \mathbf{V}_{\mathcal{S}_i^c} \underline{\boldsymbol{\epsilon}}_{\mathcal{S}_i^c} = \mathbf{V}_{\mathcal{S}_i}^\dagger \mathbf{V} \underline{\boldsymbol{\epsilon}}$. The fifth line follows from the property $\|\mathbf{A}\mathbf{x}\|_\infty \leq \|\mathbf{A}\|_\infty \|\mathbf{x}\|_\infty$. The sixth line holds because the triangle dither induces a quantization noise $\underline{\boldsymbol{\epsilon}}[n]$ whose range of amplitude is $\left(-\frac{3\lambda}{2^b}, +\frac{3\lambda}{2^b}\right)$. Consequently, $\underline{\boldsymbol{\epsilon}}[n]$ has amplitude in $\left(-\frac{6\lambda'}{2^b}, +\frac{6\lambda'}{2^b}\right)$. Finally, the last line comes from the relationship between the modulo threshold λ' and the ADC dynamic range parameter λ .

Suppose we let $M = \max_i \|\mathbf{V}_{\mathcal{S}_i}^\dagger \mathbf{V}_{\mathcal{S}_i^c}\|_\infty$. The first-order difference of the pre-estimate $\tilde{z}^{(i)}[n]$ is at most $\frac{6\lambda'}{2^b - 2} (1 + M)$

away from the first-order difference of the true residue sample. Since a rounding operation to the nearest integer multiple of $2\lambda'$ is applied to the $\tilde{z}^{(i)}[n]$ to get $\hat{z}^{(i)}[n]$, perfect recovery of $z^{(i)}[n]$ after the application of the rounding operation and equation (9) is guaranteed if

$$\frac{6\lambda'}{2^b - 2} (1 + M) < \lambda',$$

or equivalently,

$$3 + \log_2 \left(1 + \frac{3}{4}M\right) < b.$$

This is satisfied by the assumption on b stated in the theorem.

With perfect recovery of the $z^{(i)}[n]$, the terms $|z^{(i)}[n] - \hat{z}^{(i)}[n]| = 0$ for all i and n . Thus, the MSE is solely due to the quantization noise power after filtering. From Section III-B, the quantization noise power is $\mathbb{E}\{|\epsilon[n]|^2\} = \frac{1}{4} \left(\frac{2\lambda}{2^b}\right)^2$. This quantization noise power is spread evenly over the entire bandwidth $(-\pi, \pi)$ since $\epsilon[n]$ is a white process. Considering the filtering operation via a digital LPF with passband region $(-\frac{\pi}{\text{OF}} - \delta_{\text{SL}}, +\frac{\pi}{\text{OF}} + \delta_{\text{SL}})$ after the unfolding step, the power of the filtered quantization noise is only $\frac{1}{\text{OF}} + \frac{\delta_{\text{SL}}}{\pi}$ of $\mathbb{E}\{|\epsilon^{(i)}[n]|^2\}$:

$$\begin{aligned} \mathbb{E}\left\{|\epsilon_{\text{LPF}}^{(i)}[n]|^2\right\} &= \frac{\mathbb{E}\{|\epsilon^{(i)}[n]|^2\}}{\text{OF}} \left(1 + \frac{\delta_{\text{SL}} \cdot \text{OF}}{\pi}\right) \\ &= \frac{\lambda^2}{\text{OF} \cdot 2^{2b}} \left(1 + \frac{\delta_{\text{SL}} \cdot \text{OF}}{\pi}\right) \\ &= \frac{(\lambda')^2}{\text{OF} \cdot (2^b - 2)^2} \left(1 + \frac{\delta_{\text{SL}} \cdot \text{OF}}{\pi}\right). \end{aligned}$$

The proof is completed by setting $\lambda' = \frac{\|f(t)\|_\infty}{\text{OF} \cdot \left[1 - \frac{K_{\text{SL}}}{N}\right] - 2}$.

REFERENCES

- [1] Y. C. Eldar, *Sampling Theory: Beyond Bandlimited Systems*. Cambridge University Press, 2015.
- [2] C. Shannon, "Communication in the presence of noise," *Proceedings of the IRE*, vol. 37, no. 1, pp. 10–21, 1949.
- [3] T. Berger, *Rate Distortion Theory: A Mathematical Basis for Data Compression*. Englewood Cliffs, NJ, USA: Prentice-Hall, 1971.
- [4] R. Walden, "Analog-to-digital converter survey and analysis," *IEEE Journal on Selected Areas in Communications*, vol. 17, no. 4, pp. 539–550, 1999.
- [5] B. Laporte-Fauret, G. Ferré, D. Dallet, B. Minger, and L. Fuché, "Adc resolution for simultaneous reception of two signals with high dynamic range," in *2018 25th IEEE International Conference on Electronics, Circuits and Systems (ICECS)*, 2018, pp. 729–732.
- [6] A. Bhandari, F. Kraemer, and R. Raskar, "On unlimited sampling," in *2017 International Conference on Sampling Theory and Applications (SampTA)*, 2017, pp. 31–35.
- [7] A. Bhandari, F. Kraemer, and R. Raskar, "On unlimited sampling and reconstruction," *IEEE Transactions on Signal Processing*, vol. 69, pp. 3827–3839, 2021.
- [8] Y. Zhu and A. Bhandari, *Unleashing dynamic range and resolution in unlimited sensing framework via novel hardware*, 2024. arXiv: 2410.20193 [eess.SP].
- [9] R. Guo, Y. Zhu, and A. Bhandari, "Sub-nyquist usf spectral estimation: K Frequencies with $6K + 4$ modulo samples," *IEEE Transactions on Signal Processing*, vol. 72, pp. 5065–5076, 2024.
- [10] A. Bhandari, F. Kraemer, and T. Poskitt, "Unlimited Sampling From Theory to Practice: Fourier-Prony Recovery and Prototype ADC," *IEEE Trans. Signal Process.*, vol. 70, pp. 1131–1141, 2022.
- [11] E. Azar, S. Mulleti, and Y. C. Eldar, "Robust unlimited sampling beyond modulo," *arXiv preprint arXiv:2206.14656*, 2022.

- [12] Q. Zhang, J. Zhu, F. Qu, and D. W. Soh, "Line spectral estimation via unlimited sampling," *IEEE Transactions on Aerospace and Electronic Systems*, vol. 60, no. 5, pp. 7214–7231, 2024.
- [13] S. B. Shah, S. Mulleti, and Y. C. Eldar, "Lasso-based fast residual recovery for modulo sampling," in *ICASSP 2023 - 2023 IEEE International Conference on Acoustics, Speech and Signal Processing (ICASSP)*, 2023, pp. 1–5.
- [14] N. I. Bernardo, S. B. Shah, and Y. C. Eldar, "Modulo sampling with 1-bit side information: Performance guarantees in the presence of quantization," in *2024 IEEE International Symposium on Information Theory (ISIT)*, 2024, pp. 3498–3503.
- [15] M. Beckmann, A. Bhandari, and M. Iske, "Fourier-domain inversion for the modulo radon transform," *IEEE Transactions on Computational Imaging*, vol. 10, pp. 653–665, 2024.
- [16] E. Romanov and O. Ordentlich, "Above the nyquist rate, modulo folding does not hurt," *IEEE Signal Processing Letters*, vol. 26, no. 8, pp. 1167–1171, 2019.
- [17] O. Ordentlich, G. Tabak, P. K. Hanumolu, A. C. Singer, and G. W. Wornell, "A modulo-based architecture for analog-to-digital conversion," *IEEE Journal of Selected Topics in Signal Processing*, vol. 12, no. 5, pp. 825–840, 2018.
- [18] R. Guo and A. Bhandari, "Iter-sis: Robust unlimited sampling via iterative signal sieving," in *ICASSP 2023 - 2023 IEEE International Conference on Acoustics, Speech and Signal Processing (ICASSP)*, 2023, pp. 1–5.
- [19] A. Bhandari, F. Krahermer, and R. Raskar, "Unlimited sampling of sparse signals," in *2018 IEEE International Conference on Acoustics, Speech and Signal Processing (ICASSP)*, 2018, pp. 4569–4573.
- [20] O. Musa, P. Jung, and N. Goertz, "Generalized approximate message passing for unlimited sampling of sparse signals," in *2018 IEEE Global Conference on Signal and Information Processing (GlobalSIP)*, 2018, pp. 336–340.
- [21] V. Shah and C. Hegde, "Sparse signal recovery from modulo observations," *EURASIP Journal on Advances in Signal Processing*, vol. 2021, no. 1, pp. 1–17, 2021.
- [22] D. Prasanna, C. Sriram, and C. R. Murthy, "On the identifiability of sparse vectors from modulo compressed sensing measurements," *IEEE Signal Processing Letters*, vol. 28, pp. 131–134, 2021.
- [23] L. GAN and H. Liu, "High dynamic range sensing using multi-channel modulo samplers," in *2020 IEEE 11th Sensor Array and Multichannel Signal Processing Workshop (SAM)*, 2020, pp. 1–5.
- [24] Y. Gong, L. Gan, and H. Liu, "Multi-channel modulo samplers constructed from gaussian integers," *IEEE Signal Processing Letters*, vol. 28, pp. 1828–1832, 2021.
- [25] G. Shtendel and A. Bhandari, "Dual-channel unlimited sampling for bandpass signals," in *ICASSP 2024 - 2024 IEEE International Conference on Acoustics, Speech and Signal Processing (ICASSP)*, 2024, pp. 9711–9715.
- [26] D. Florescu, "Multichannel modulo sampling with unlimited noise," in *ICASSP 2025 - 2025 IEEE International Conference on Acoustics, Speech and Signal Processing (ICASSP)*, 2025, pp. 1–5.
- [27] D. Florescu, F. Krahermer, and A. Bhandari, "Unlimited sampling with hysteresis," in *2021 55th Asilomar Conference on Signals, Systems, and Computers*, 2021, pp. 831–835.
- [28] D. Florescu, F. Krahermer, and A. Bhandari, "The surprising benefits of hysteresis in unlimited sampling: Theory, algorithms and experiments," *IEEE Transactions on Signal Processing*, vol. 70, pp. 616–630, 2022.
- [29] D. Florescu and A. Bhandari, "Unlimited sampling via generalized thresholding," in *2022 IEEE International Symposium on Information Theory (ISIT)*, 2022, pp. 1606–1611.
- [30] D. Florescu and A. Bhandari, "Unlimited sampling with local averages," in *ICASSP 2022 - 2022 IEEE International Conference on Acoustics, Speech and Signal Processing (ICASSP)*, 2022, pp. 5742–5746.
- [31] G. Joseph, "Noise-resilient unlimited sampling and recovery of sparse signals," in *ICASSP 2025 - 2025 IEEE International Conference on Acoustics, Speech and Signal Processing (ICASSP)*, 2025, pp. 1–5.
- [32] A. Krishna, S. Rudresh, V. Shaw, H. R. Sabbella, C. S. Seelamantula, and C. S. Thakur, *Unlimited dynamic range analog-to-digital conversion*, 2019. arXiv: 1911.09371 [eess.SP].
- [33] S. Fernández-Menduiña, F. Krahermer, G. Leus, and A. Bhandari, "Computational array signal processing via modulo non-linearities," *IEEE Transactions on Signal Processing*, vol. 70, pp. 2168–2179, 2022.
- [34] S. Mulleti, E. Reznitskiy, S. Savariego, M. Namer, N. Glazer, and Y. C. Eldar, "A hardware prototype of wideband high-dynamic range analog-to-digital converter," *IET Circuits, Devices & Systems*, vol. 17, no. 4, pp. 181–192, 2023. eprint: <https://ietresearch.onlinelibrary.wiley.com/doi/pdf/10.1049/cds2.12156>.
- [35] J. Zhu, J. Ma, Z. Liu, F. Qu, Z. Zhu, and Q. Zhang, *A modulo sampling hardware prototype and reconstruction algorithm evaluation*, 2024. arXiv: 2410.19383 [eess.SP].
- [36] S. B. Shah, S. Mulleti, and Y. C. Eldar, "Compressed sensing based residual recovery algorithms and hardware for modulo sampling," *arXiv preprint arXiv:2412.12724*, 2024.
- [37] A. Bhandari and F. Krahermer, "Hdr imaging from quantization noise," in *2020 IEEE International Conference on Image Processing (ICIP)*, 2020, pp. 101–105.
- [38] L. G. Ordoñez, P. Ferrand, M. Duarte, M. Guillaud, and G. Yang, "On full-duplex radios with modulo-adcs," *IEEE Open Journal of the Communications Society*, vol. 2, pp. 1279–1297, 2021.
- [39] T. Feuillen, M. Alaee-Kerahroodi, A. Bhandari, B. S. M. R, and B. Ottersten, "Unlimited sampling for fmcw radars: A proof of concept," in *2022 IEEE Radar Conference (RadarConf22)*, 2022, pp. 1–5.
- [40] T. Feuillen, B. Shankar MRR, and A. Bhandari, "Unlimited sampling radar: Life below the quantization noise," in *ICASSP 2023 - 2023 IEEE International Conference on Acoustics, Speech and Signal Processing (ICASSP)*, 2023, pp. 1–5.
- [41] G. Shtendel, D. Florescu, and A. Bhandari, "Unlimited sampling of bandpass signals: Computational demodulation via undersampling," *IEEE Transactions on Signal Processing*, vol. 71, pp. 4134–4145, 2023.
- [42] T. Geng, F. Ji, Pratibha, and W. P. Tay, "Modulo eeg signal recovery using transformer," in *ICASSP 2023 - 2023 IEEE International Conference on Acoustics, Speech and Signal Processing (ICASSP)*, 2023, pp. 1–5.
- [43] Z. Liu, A. Bhandari, and B. Clerckx, " λ -mimo: Massive mimo via modulo sampling," *IEEE Transactions on Communications*, vol. 71, no. 11, pp. 6301–6315, 2023.
- [44] Z. Liu, A. Bhandari, and B. Clerckx, "Full-duplex beyond self-interference: The unlimited sensing way," *IEEE Communications Letters*, vol. 29, no. 1, pp. 165–169, 2025.
- [45] Q. Zhang, J. Zhu, F. Qu, and D. W. Soh, "One-bit-aided modulo sampling for doa estimation," in *2025 International Radar Conference*, 2025.
- [46] S. Mulleti, K. Appaiiah, and S. R. B. Pillai, "Low-rate modulo folded adc for detecting linearly modulated communication symbols," in *ICASSP 2025 - 2025 IEEE International Conference on Acoustics, Speech and Signal Processing (ICASSP)*, 2025, pp. 1–5.
- [47] A. Eamaz, K. V. Mishra, F. Yeganegi, and M. Soltanalian, "Uno: Unlimited sampling meets one-bit quantization," *IEEE Transactions on Signal Processing*, vol. 72, pp. 997–1014, 2024.
- [48] N. I. Bernardo, S. B. Shah, and Y. C. Eldar, "Modulo sampling: Performance guarantees in the presence of quantization," *IEEE Transactions on Signal Processing*, pp. 1–14, 2025.
- [49] J. Rhee and Y. Joo, "Wide dynamic range cmos image sensor with pixel level adc," *Electronics Letters*, vol. 39, pp. 360–361, Mar. 2003.
- [50] K. Sasagawa, T. Yamaguchi, M. Haruta, et al., "An implantable cmos image sensor with self-reset pixels for functional brain imaging," *IEEE Transactions on Electron Devices*, vol. 63, no. 1, pp. 215–222, 2016.
- [51] MathWorks. "Tukey window." Accessed: 2024-9-23. (2024), [Online]. Available: <https://www.mathworks.com/help/signal/ref/tukeywin.html>.
- [52] R. Gray and T. Stockham, "Dithered quantizers," *IEEE Transactions on Information Theory*, vol. 39, no. 3, pp. 805–812, 1993.
- [53] Q. Zhang, J. Zhu, F. Qu, Z. Zhu, and D. W. Soh, *On the identifiability from modulo measurements under dft sensing matrix*, 2024. arXiv: 2401.00194 [cs.IT].
- [54] K. Itoh, "Analysis of the phase unwrapping algorithm," *Appl. Opt.*, vol. 21, no. 14, pp. 2470–2470, Jul. 1982.
- [55] O. Graf, A. Bhandari, and F. Krahermer, "One-bit unlimited sampling," in *ICASSP 2019 - 2019 IEEE International Conference on Acoustics, Speech and Signal Processing (ICASSP)*, 2019, pp. 5102–5106.